Supporting Information

Characterizations. The crystal phase of both freshly synthesized powders were detected by X-ray diffraction (XRD, Bruker AXS D8-Focus, Germany) with Cu Kα radiation in the range of 2θ from 10 º to 80 º. The micromorphology of NiCo-LDH and Fe^{EP}-NiCo-LDH powders were observed by means of a field emission scanning electron microscopy (FESEM, Hitch SU8010, Japan). The X-ray photoelectron spectroscopy (XPS, Escalab 250XI, ThermoFisher, USA) was employed to further explore the composition, chemical environment and surface electronic state of the samples. All XPS profiles are aligned by C 1s (284.60 eV). The transmission electron microscope (TEM) and high-resolution transmission electron microscope (HR-TEM) images were observed under JEM-2100F field emission transmission electron microscopy. The metal element content of all samples were measured by Inductively coupled plasma mass spectrometry (ICP-MS).

Product analysis. Nuclear magnetic resonance (Ascend 600) was used to analyze the product content of the methanol oxidation reaction. First, a series of potassium formate (HCOOK) solutions of different concentrations (1 mM, 3 mM, 5 mM, 7 mM, 10 mM, 15 mM, 20 mM) were prepared. 500 μL of potassium formate solution and 100 μLof D_2O (containing 0.05 wt% TMSP) were added into a NMR tube and mixed thoroughly for NMR test. A standard curve was drawn based on the proportional relationship between the integrated intensity of the formate ion signal peak and the concentration of formate ion. Typically, for the analysis of the product in the electrolyte, 500 μL of electrolyte and 100 μL of D_2O (containing 0.05 wt% TMSP) were added in a NMR tube and mix them thoroughly. Then the nuclear magnetic resonance test was performed to obtain the integrated intensity ofthe formate ion signal. The content of formate produced was calculated according to the standard curve.

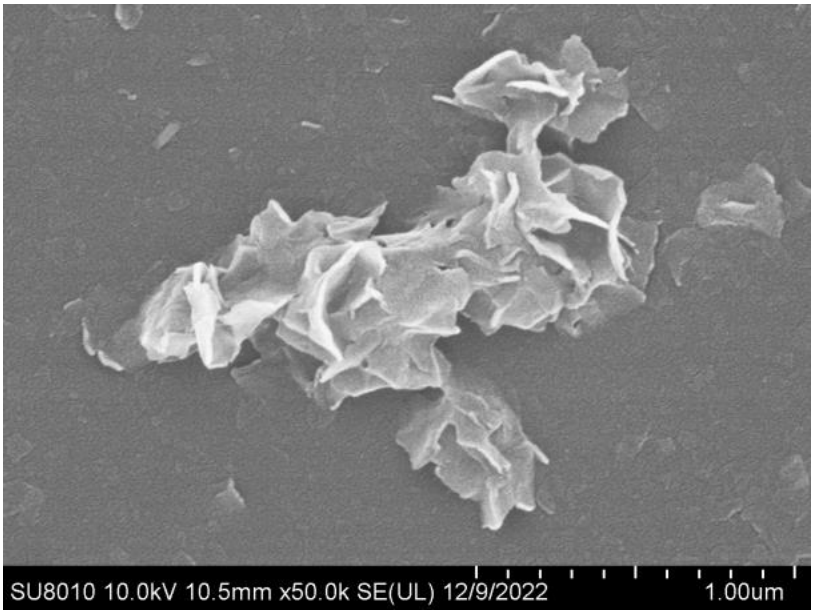

Figure S1. The SEM image of NiCo-LDH catalyst.

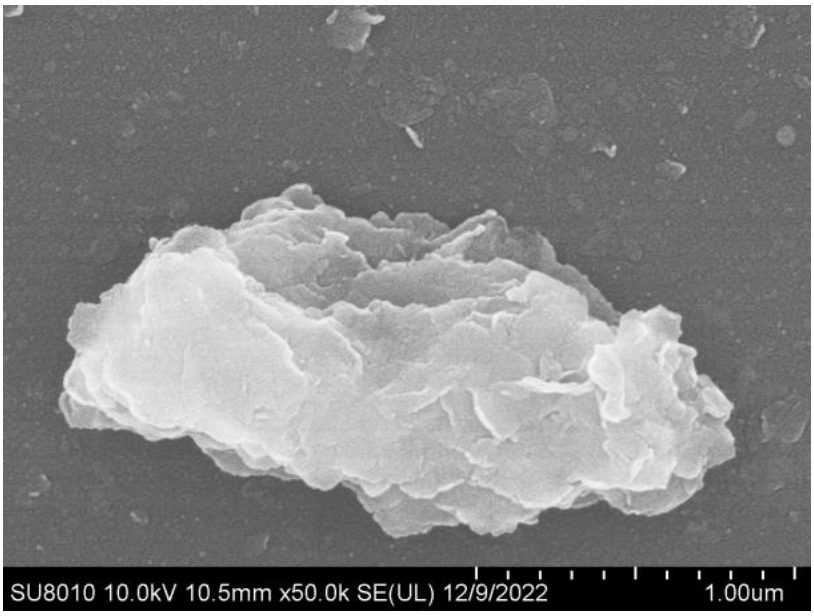

Figure S2. The SEM image of Fe^{EP}-NiCo-LDH catalyst.

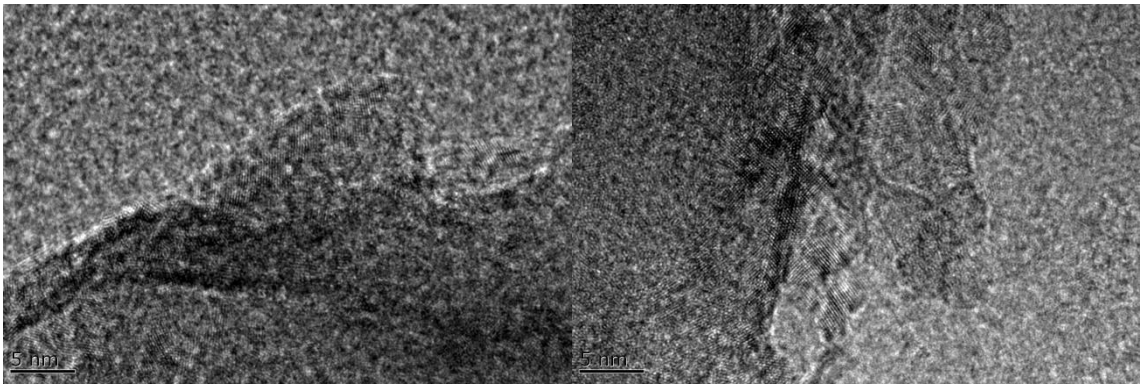

Figure S3. The TEM images of Fe^{EP}-NiCo-LDH catalyst.

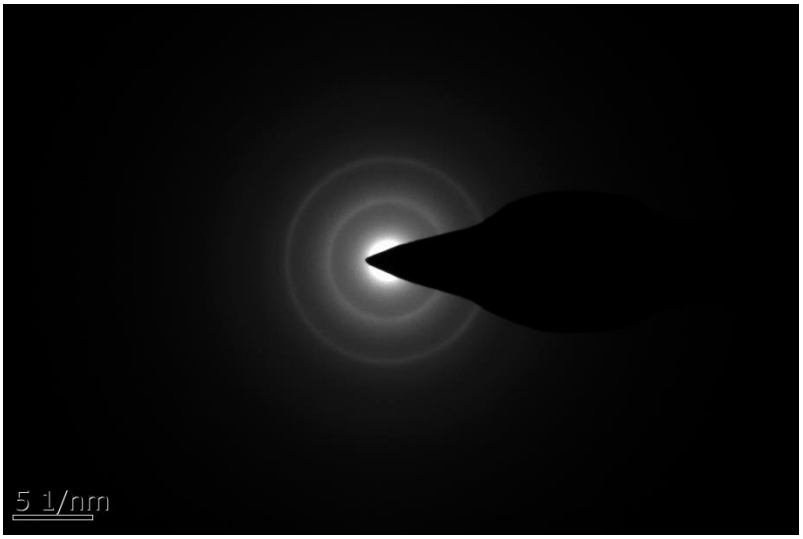

Figure S4. The selected area electron diffraction (SAED) of Fe^{EP}-NiCo-LDH.

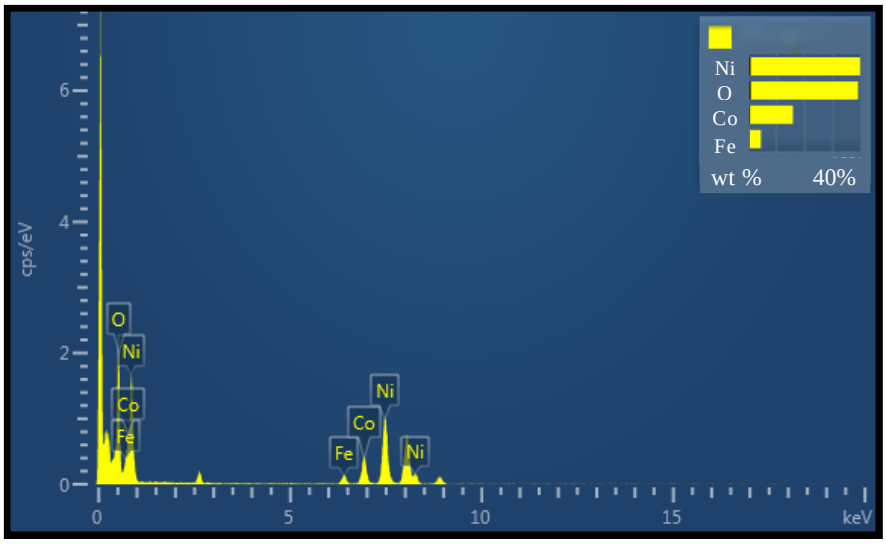

Figure S5. The atomic ratios of Fe^{EP}-NiCo-LDH catalyst.

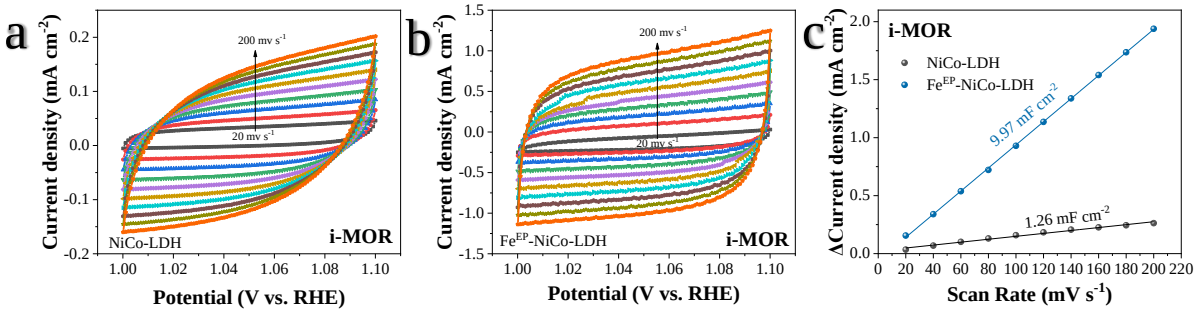

Figure S6. Cyclic voltammograms with different sweeping rates from 20 to 200 mV s^{-1} in the potential range of 1.0-1.1 V in 1M KOH and 1M MeOH solution on (a) the NiCo-LDH, (b) the Fe^{EP}-NiCo-LDH and the electrochemical double-layer capacitances of the i-MOR on the NiCo-LDH and Fe^{EP}-NiCo-LDH catalysts.

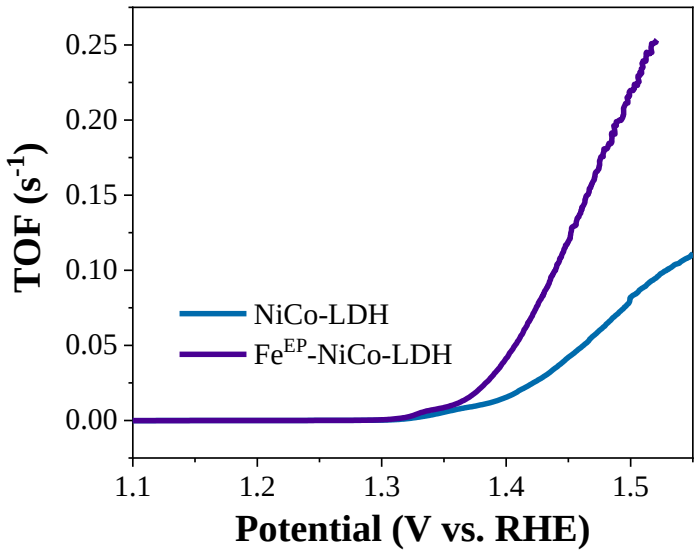

Figure S7. The TOF curves of NiCo-LDH and Fe^{EP}-NiCo-LDH catalysts.

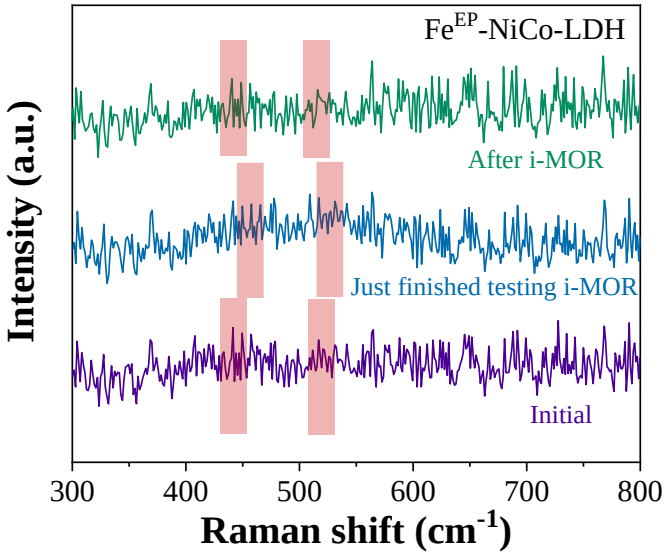

Figure S8. Before and after i-MOR test, the Raman spectroscopy of Fe^{EP}-NiCo-LDH catalyst.

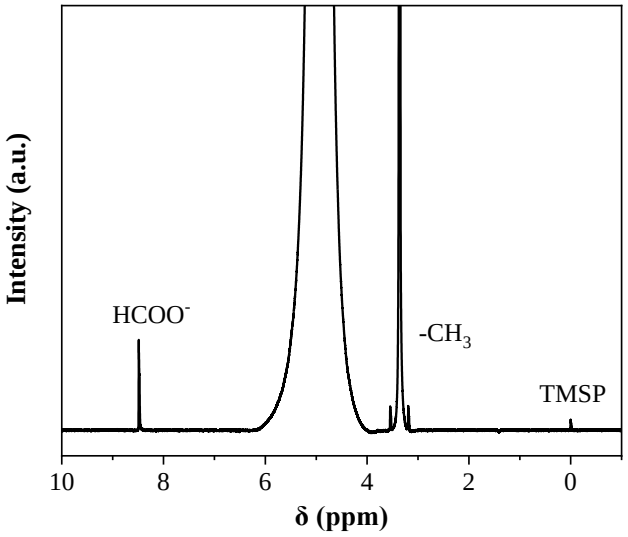

Figure S9. A 1H NMR spectrum of the electrolyte after i-MOR.

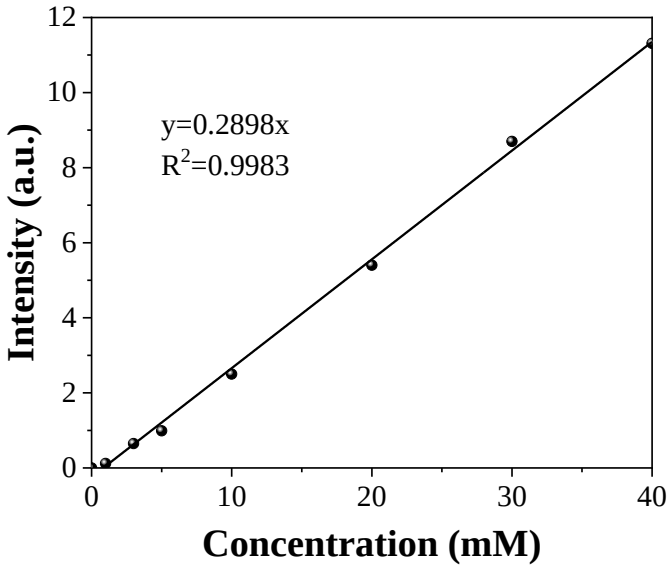

Figure S10. Standard curve for formate quantification.

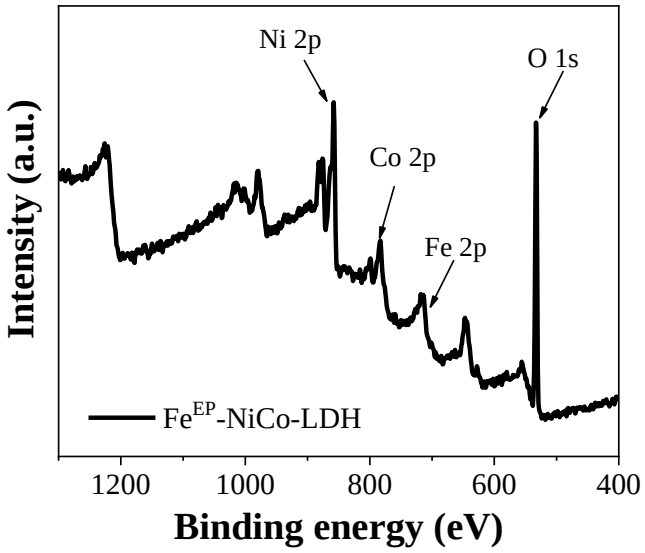

Figure S11. The full XPS spectra of Fe^{EP}-NiCo-LDH catalyst.

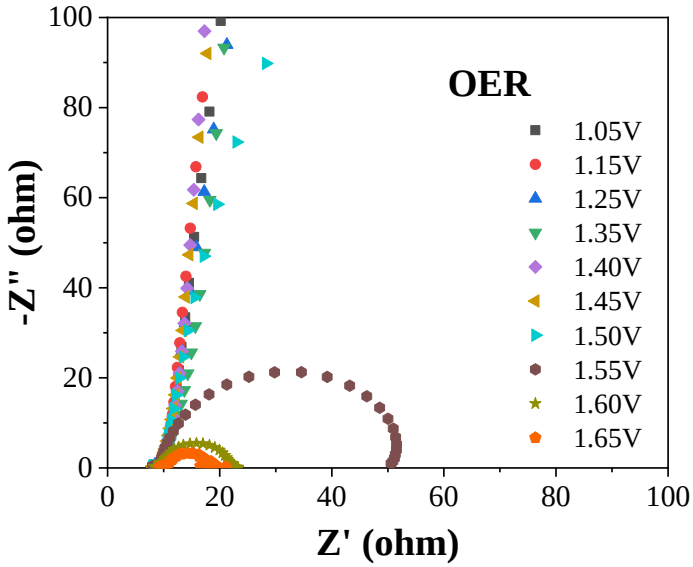

Figure S12. The Nyquist plots of NiCo-LDH catalyst at different potentials in 1M KOH.

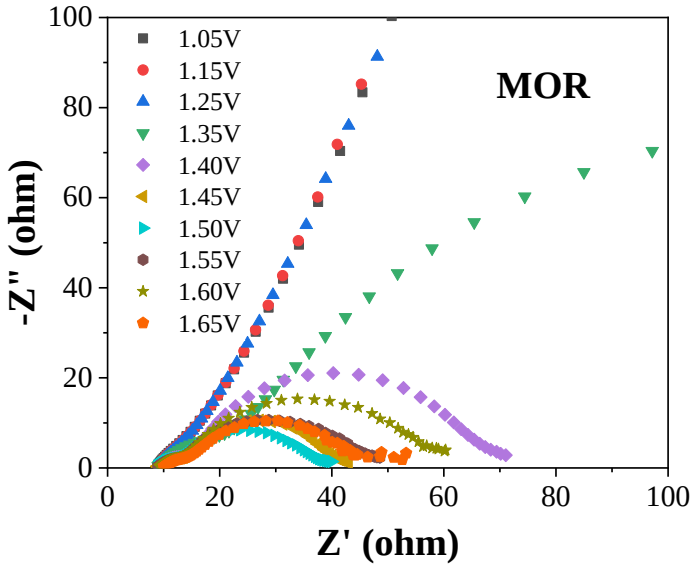

Figure S13. The Nyquist plots of NiCo-LDH catalyst at different potentials in 1M KOH with 1M MeOH.

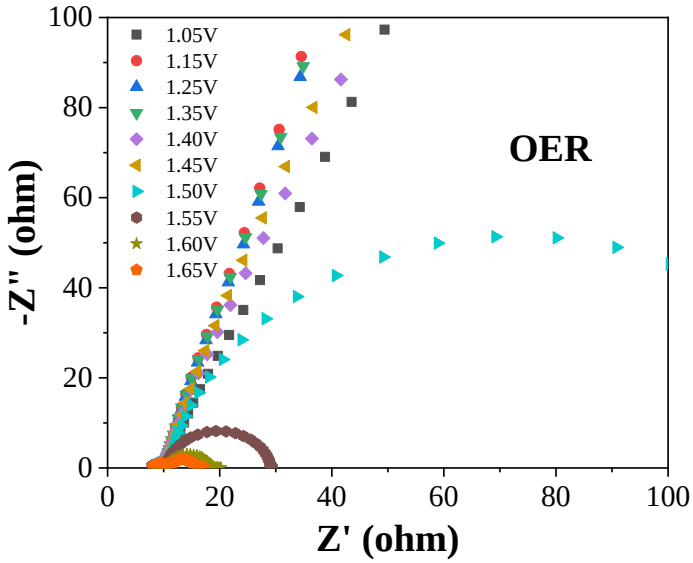

Figure S14. The Nyquist plots of Fe^{EP}-NiCo-LDH catalyst at different potentials in 1M KOH.

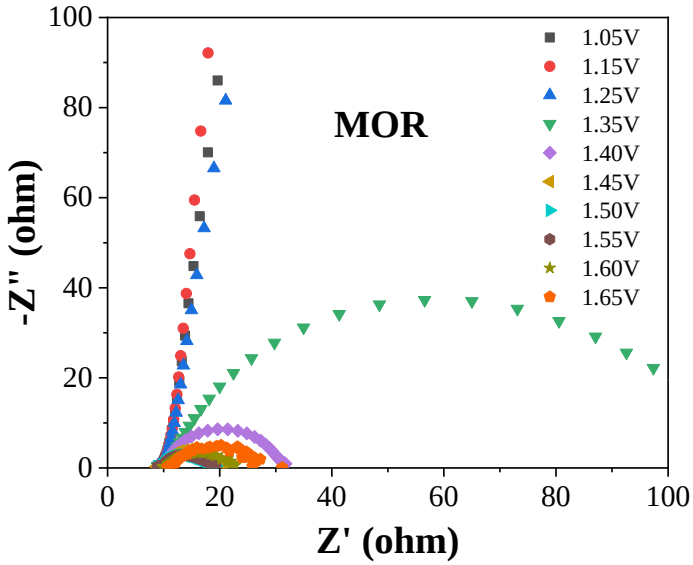

Figure S15. The Nyquist plots of NiCo-LDH catalyst at different potentials in 1M KOH.

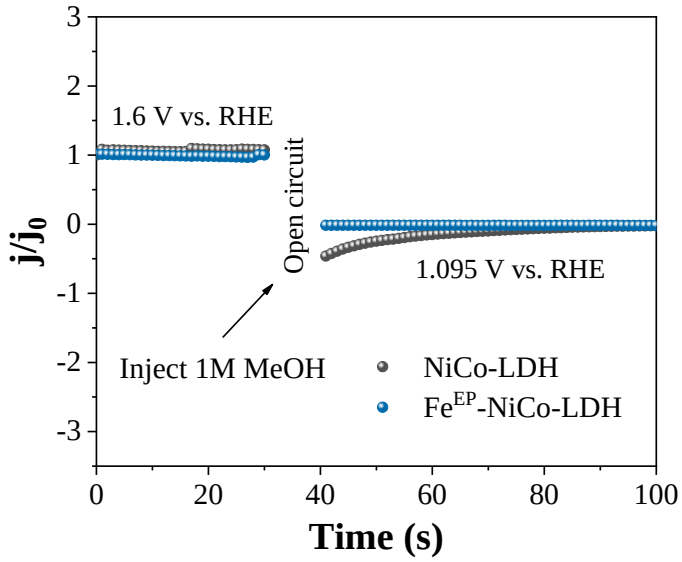

Figure S16. Multi-potential step curves of NiCo-LDH and Fe^{EP}-NiCo-LDH (including 5 s open circuit time).

Table S1. Atomic ratios of Fe^{EP}-NiCo-LDH catalyst.

Element	Ni	Co	Fe	O
Atomic ratio (at.%)	19.49	7.84	2.45	70.22

Table S2. The metal elements content of NiCo-LDH and Fe^{EP}-NiCo-LDH catalysts tested by ICP-MS.

Catalyst	Ni (wt%)	Co (wt%)	Fe (wt%)
NiCo-LDH	40.05	16.78	-
Fe^{EP}-NiCo-LDH	39.51	15.36	3.64

Table S3. Comparison of recently reported Ni-based electrocatalysts for i-MOR.

Electrocatalyst	MOR performance	Tafel slope	Electrolyte	FE of oxidation product	Product	Ref
Fe^{EP}-NiCo-LDH	1.349/1.430 V at 10/100 mA cm^{-2}	29.1 mV dec^{-1}	1 M KOH+1 M MeOH	~95%	Formate	This work
NiCo/ N-TiO_2 @NaOH	1.5 V at 73 mA cm^{-2}	59 mV dec^{-1}	1 M KOH+1 M MeOH	-	-	[1]
NiFe LDH@SnO_2/NF	1.396 V at 10 mA cm^{-2}	22.4 mV dec^{-1}	1 M KOH+0.5 M MeOH	-	Formate	[2]
NiP_x-R	1.49 V at 100 mA cm^{-2} (CV)	39.4 mV dec^{-1}	1 M KOH+0.5 M MeOH	-	Formate	[3]
NiB-400	1.54 V at 500 mA cm^{-2}	-	1 M KOH+1 M MeOH	~100%	Formate	[4]
NiMn-LDH	1.41 V at 100 mA cm^{-2}		1 M KOH+3 M MeOH	~100%	Formate	[5]
CNFs/NiSe/CC	1.51 V at 100 mA cm^{-2}	24 mV dec^{-1}	1 M KOH+1 M MeOH	97.9%	Formate	[6]

1. S. Zhao, T. Wang, Z. Ji, Y. Song, Y. Li, J. Liu and W. Hu, *Appl. Catal. B*, 2023, **320**.
2. C. Wan, J. Jin, X. Wei, S. Chen, Y. Zhang, T. Zhu and H. Qu, *J Mater Sci Technol*, 2022, **124**, 102-108.
3. S. Li, R. Ma, J. Hu, Z. Li, L. Liu, X. Wang, Y. Lu, G. E. Sterbinsky, S. Liu, L. Zheng, J. Liu, D. Liu and J. Wang, *Nat Commun*, 2022, **13**, 2916.
4. Y. Qi, Y. Zhang, L. Yang, Y. Zhao, Y. Zhu, H. Jiang and C. Li, *Nat Commun*, 2022, **13**, 4602.
5. B. Zhu, B. Dong, F. Wang, Q. Yang, Y. He, C. Zhang, P. Jin and L. Feng, *Nat Commun*, 2023, **14**, 1686.
6. B. Zhao, J.-W. Liu, Y.-R. Yin, D. Wu, J.-L. Luo and X.-Z. Fu, *J. Mater. Chem. A*, 2019, **7**, 25878-25886.